We are IntechOpen, the world's leading publisher of Open Access books Built by scientists, for scientists

4,800
Open access books available

122,000
International authors and editors

135M
Downloads

Our authors are among the

154
Countries delivered to

TOP 1%
most cited scientists

12.2%
Contributors from top 500 universities

CLARIVATE ANALYTICS BOOK CITATION INDEX INDEXED

WEB OF SCIENCE™

Selection of our books indexed in the Book Citation Index in Web of Science™ Core Collection (BKCI)

Interested in publishing with us?
Contact book.department@intechopen.com

Numbers displayed above are based on latest data collected.
For more information visit www.intechopen.com

14

New Concepts of Integrated Photonic Biosensors Based on Porous Silicon

Cécile Jamois[1] et al*
[1]*Institut des Nanotechnologies de Lyon (INL), CNRS UMR 5270, INSA-Lyon*
[2]*Institut des Nanotechnologies de Lyon (INL), CNRS UMR 5270, Ecole Centrale de Lyon*
Université de Lyon
France

1. Introduction

A biosensor is a device that uses specific biochemical reactions mediated by isolated tissues, enzymes, immunosystems, organelles or whole cells to detect chemical compounds (IUPAC: http://goldbook.iupac.org/B00663.html). Biosensors integrate two functions, i) a bio-receptor functionalized with probes able to specifically recognize the targeted species and ii) a transducer converting the specific biological interaction into a quantitatively measurable signal. One way to classify biosensors relates on the transduction mode, such as optical (fluorescence, surface-enhanced Raman scattering, chemiluminescence, colorimetry, dual polarization interferometry and surface plasmon resonance), electrochemical (amperometry, potentiometry, field-effect transistor and conductimetry) and gravimetric transduction (quartz crystal microbalance, cantilever) (Sassolas et al., 2008).
The evaluation of biosensor performances relies on the following criteria: high sensitivity, operational and linear concentration range, detection and quantitative determination limits, high selectivity, steady-state and transient response times, sample throughput, reliability, reproducibility, stability and long lifetime (Thévenot et al., 1999). Other aspects like cost of test, ease of use, time of analysis including all the steps required for sample preparation should also be taken into account. Some biosensors are based on the use of labels such as colorimetric, fluorescent, enzymatic moieties or redox species... However, the current trends aim to develop on-chip integrated and label free detection systems. In this framework, porous silicon (PSi) offers high potential for biosensing:

- PSi physical properties directly depend on the structure. The optical properties are linked to the variation of refractive index with a change of porosity while the electrochemical properties rely on surface chemistry modification. Thus, PSi based transducers can be sensitive both to surface or volume biomolecular recognition.
- PSi surface chemistry is essentially governed by the high reactivity of Si-H bond, which can form both Si-alkyle or Si-OH bond (Stewart & Buriak, 2000). Thus, the surface can be either hydrophobic or hydrophilic, and a large range of biomolecules can be immobilized.

*Cheng Li[1], Emmanuel Gerelli[1], Régis Orobtchouk[1], Taha Benyattou[1], Ali Belarouci[2], Yann Chevolot[2], Virginie Monnier[2] and Eliane Souteyrand[2]

- The porosity of PSi can vary from 15 to 90%, yielding high specific surface and pore size ranging from nanopores (< 2 nm) to macropores (> 50 nm) (Canham, 1990). Mesopores (with 2-50 nm diameter) are the most suitable for biosensing, because they are large enough to allow for good biomolecule diffusion and they yield large specific surfaces ranging from 100 m^2/g to 350 m^2/g, which strongly increases the amount of biomolecules that can be immobilized on the transducer compared to a 2D surface immobilization. It is worthwhile to point out that the accessibility of the probes by the target molecules (to be detected) depends both on the pore size and on the surface energy of PSi (Tinsley-Bown et al., 2000).
- Finally, PSi is fully compatible with standard microprocessing techniques and can be micromachined, etched, and on-chip integrated.

The scope of this chapter is to present new concepts of integrated PSi biosensors, as well as the tools used for their study and realization, and a discussion on their performances.

2. Biosensors based on porous silicon

In the field of biosensors, PSi is mainly used for its large surface area. As an example, functionalized PSi was used in a modified single-tube format chemiluminescent assay to catalyze an enzymatic reaction indicating the presence of *Escherichia coli* bacteria. A lower detection limit of 10 cells within 40 min was obtained using PSi, compared to 10^3 cells for "classical" tube chemiluminescence assay (Mathew & Alocija, 2005). PSi thin films functionalized with covalently grafted antibodies were also used to selectively capture dye-labelled MS2 bacteriophage viruses (Rossi et al., 2007). Although pore penetration and binding efficiency depend on PSi surface wettability, fluorescence measurements showed a detection limit of $2x10^7$ pfu/ml (pfu: plaque-forming units) and a dynamic range for the measurement of viral concentrations from $2x10^7$ to $2x10^{10}$ pfu/ml. In these two cases, the targeted species are detected by chemiluminescent or fluorescent intensity measurements.

Biosensors can be advantageously based on electrical or electrochemical transducer properties when the biological recognition involves the conversion of an electroactive substance in contact with the target to be detected, e.g., in the case of enzymatic reaction. The current generated by electron transfer can be directly measured by amperometry if a conductive working electrode is used. A limiting factor for the sensitivity and the dynamic range is the amount of catalyzing species entrapped at the surface of the working electrode. Hence, a way to improve amperometric biosensor performances is the enlargement of the electrode area. Using a platinum-coated PSi layer to determine cholesterol concentration, a 3-fold increase of sensitivity was obtained compared to a planar electrode (Song et al. 2006).

A second class of electrical biosensors takes advantage of the semiconducting properties of Si substrates. In 1970, it was shown that a Field Effect Transistor (FET) can be adapted to work in aqueous media to build a so-called ISFET device that is sensitive to the ionic interactions with the SiO_2 surface (Bergveld, 1970). In the ENFET proposed in 1980, the sensing surface of FET is modified with enzymatic species (Caras & Janata, 1980). In 1994, we proposed the GENFET, a device using the intrinsic properties of negatively charged DNA strands for in-situ and direct label-free detection of DNA hybridization (Martin et al., 1994). In order to detect simultaneously different DNA sequences, we showed that the photopotential of electrolyte/SiO_2/Si semiconducting device is sensitive to the variation of the surface charge induced by DNA hybridization and could be used as a transducer for DNA chips (Souteyrand et al., 1997, 2000). In 1996, a PSi layer was added at the surface of

the bulk Si potentiometric device to measure penicillin concentration. An enlarged linear range of the calibration curve and higher signals were obtained, which were attributed to the larger amount of enzyme immobilised on the PSi substrate compared to planar structures (Thust et al., 1996, 1999). To conclude, in the case of electrical transducers, the improvement of biosensor performances achieved with PSi layers is usually only due to an increase of the specific working area and not to improvement of the electrical properties.

In the case of label-free optical detection, biosensors exploit the refractive index variations induced by the presence of target biomolecules specifically bound to probes immobilized at the sensor surface. Among the large family of PSi optical biosensors, the simplest devices are Fabry-Perot interferometers constituted of a few µm-thick PSi monolayers. Large shifts of the interference fringes induced by the binding of target molecules have been observed for a large variety of molecules such as DNA, proteins or small organic biomolecules (Lin et al., 1997). Multilayer structures exhibiting high reflectivity in well-defined frequency ranges, such as Bragg mirrors (Rendina et al., 2007) or rugate filters (Chapron et al., 2007; Cunin et al., 2002), have also been widely studied for biosensing applications. These devices usually yield increased sensitivity due to multiple reflections of light within the multilayers, which enhance light-matter interactions. When a layer is introduced inside the multilayer structure with a different width or a different porosity from the PSi layers constituting the multilayer, a microcavity is built. Such a device enables to obtain very narrow resonances that are highly confined inside the microcavity and thus are very sensitive to any variation in refractive index induced by the presence of target biomolecules in this layer. It has been demonstrated that molecule layers as thin as 0.01 nm could be detected using microcavities (Ouyang et al., 2006). These devices are also suitable for antibodies detection in whole blood samples with high specificity and good sensitivity (Bonanno & DeLouise, 2007).

As an alternative to biosensors based on multilayers, planar waveguides have also been proposed. They consist of a thin waveguiding layer with medium porosity on top of a highly porous substrate. Contrary to interferometers or multilayers that are usually used at normal incidence, planar waveguides support light modes that are propagating within the waveguide parallel to the surface. These modes are confined by total internal reflection due to the refractive index difference between the waveguide and the surrounding air or the highly porous substrate, respectively. In order to excite such propagating modes, light is usually coupled through a prism at very particular incidence angles. Refractive index variation in the waveguide layer can be observed by monitoring the variation in coupling angle. Very high sensitivities corresponding to detection limits of 5 pg/mm^2 have been reported using such sensors for DNA detection (Rong et al., 2008).

In the PSi-based optical biosensors cited above, red shifts are usually expected because the presence of the target biomolecules should increase the PSi refractive index. However, it has been demonstrated that a competing mechanism can lead to strong blue shifts. If Si-H or Si-OH bonds are present on the PSi surface, a transfer of negative charges from the bound molecules to the PSi can catalyze oxidation by the surrounding water molecules and results in strong corrosion of the PSi, thus in strong reduction of refractive index. The resulting blue shifts have often been observed in the case of DNA hybridization (Lin et al., 1997), and DNA biosensors based on catalytic corrosion were proposed and shown to yield much higher sensitivities than red-shift sensors (Steinem et al., 2004). The transduction mechanism was recently generalized to non-charged molecules by oxidation hydrolysis via metal catalysts in presence of oxidants, and avidin detection on biotinized PSi surfaces was demonstrated

(Völcker et al., 2008). It is important to point out that this type of biosensors is restricted to single-use, as the corrosion leads to destruction of the PSi structure.
More complete reviews on PSi-based biosensors (Jane et al., 2009) or on label-free optical biosensors (Fan et al., 2008) can be found in the literature.

3. Novel photonic-crystal-based biosensors

As presented above, most PSi optical sensors share the particularity that their active region for sensing is either buried – e.g., micro-cavities in multilayers – or very thick – as in the case of interferometric devices. This leads to limitations of the diffusion of biomolecules inside the porous structure, which introduce delays in the device response and alter the optical properties due to in-depth inhomogeneity of infiltration. These issues can be reduced if the sensing layer is at the device surface and relatively thin, as in the case of planar waveguides.
The sensitivity of such planar sensors could be greatly enhanced if the surface configuration of planar waveguides could be combined with stronger light confinement and/or strong slowing down of light in order to increase light-matter interactions. The use of gratings (Ryckman et al., 2010) constitutes a first step towards improving the optical properties. Another way is to design new sensors using photonic crystals (PCs) concepts.
Photonic crystals are periodic arrangements of dielectric media (Joannopoulos et al., 1995; Viktorovitch et al., 2007, 2010). The periodicity can be either along one direction for one-dimensional (1D) PCs, in a plane for two-dimensional (2D) PCs, or in all dimensions for three-dimensional (3D) PCs. In this sense, periodic multilayers such as Bragg mirrors constitute 1D PCs. PCs have the great property to exhibit band structures for photons, i.e., light in such structures can only have discrete frequency states called photonic bands. Convenient engineering of photonic bands enables to control light velocity. Moreover, photonic band gaps (PBGs) can exist, i.e., frequency regions where light propagation is prohibited inside the PC. Hence, through a careful design of the PC it is possible to tailor its optical properties in order to strongly confine light in a given region of the device and to strongly reduce its propagation velocity.
In the following, we will present two different concepts of planar biosensors using PCs properties to increase sensitivity: a surface wave biosensor and a planar 1D PC device.

3.1 Surface-wave biosensor

The surface wave (SW) biosensor consists of a periodic multilayer with a defect layer at its surface. It can be understood as a hybrid between a planar waveguide and a microcavity device. Similarly to the planar waveguide, light can be excited within the PSi structure, e.g. through a prism, and confined due to the refractive index contrast between the dielectric structure and the lower-index environment. Similarly to the microcavity sensor, the periodic multilayer exhibits a PBG which prohibits light propagation inside the multilayer. Hence, light excited in such a device is forced to propagate within the thin defect top layer, leading to very strong light confinement and intensity within this surface layer. The sensitivity of SW devices has already been demonstrated for sensing applications (Liscidini & Sipe, 2007; Shinn & Robertson, 2005). It can be enhanced further if the devices are made in a material with much greater specific surface like PSi (Guillermain et al., 2006, 2007).
The principle of the SW biosensor is illustrated in fig. 1. Light is coupled to the PSi device through a prism. In this configuration, the SW can only be excited at a given frequency for a particular angle of incidence θ_0, when its wave vector is matching the parallel wave vector

of the incident beam inside the prism. At the particular angle of incidence θ_0, most light is coupled to the SW, leading to a strong intensity decrease of the reflected beam. As the coupling conditions to the SW strongly depend on the surface layer configuration, in particular its refractive index, any change in refractive index induced by the presence of the target molecules should lead to a variation of the coupling angle, as illustrated in fig. 1b.

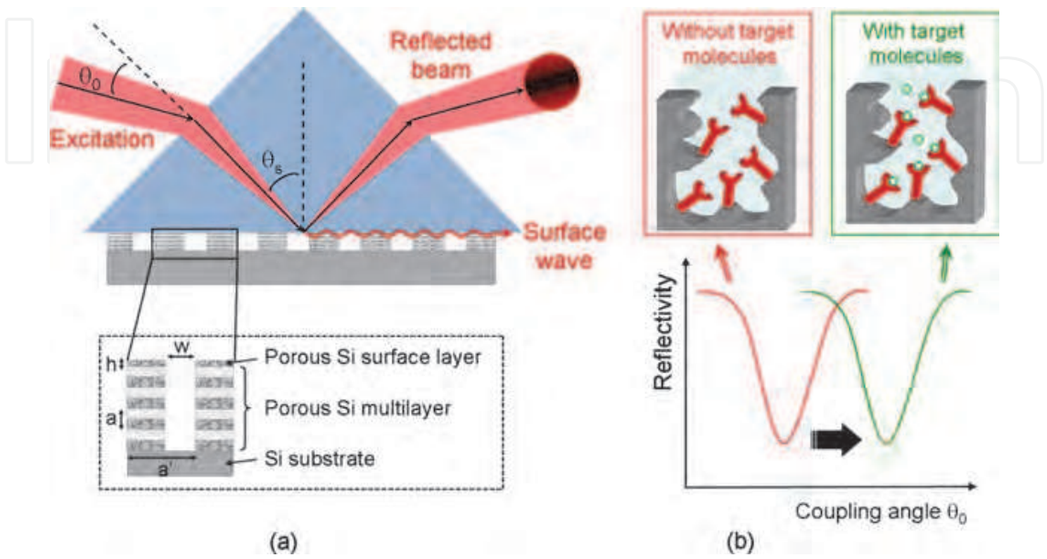

Fig. 1. Principle of the surface wave sensor: (a) device description, and (b) principle of optical sensing.

When compared to planar waveguides, the SW device presents the great advantage that the top layer can be of any porosity, provided that the layer thickness is correspondingly adjusted to optimize the optical properties. This means that the porosity of the top layer can be chosen depending on the size and properties of the biomolecules to detect. This is not the case in planar waveguides where the porosity of the top layer is limited, since the refractive index of the waveguide should be higher than that of the underlying PSi substrate. Moreover, we will demonstrate in section 6.1 that strong decrease of light velocity can be achieved via a lateral patterning of the multilayer with air slits as shown in fig. 1a, leading to strong enhancement of the biosensor sensitivity (Jamois et al., 2010a).
In the configuration shown in fig. 1a, the surface of the PSi device is facing the prism. In the case where in-situ experiments should be performed, the same biosensor could be used, provided that it is reported onto a transparent substrate in order to couple light from the backside and leave the PSi device in contact with the analyte.

3.2 Planar photonic-crystal biosensor

The planar 1D PC biosensor consists of a PSi layer with low or medium porosity on top of a higher-porosity substrate. As illustrated in fig. 2a, the top layer is patterned by a periodic array of air slits that extend in the depth down to the underlying porous substrate. When excited by a light beam at normal incidence, such a device can support particular modes, called Fano resonances that result from the coupling between the discrete bands of the 1D PC and the continuous states of the surrounding medium seen by the incident beam. These resonances are highly confined within the top layer and can have very high spectral finesse

(Jamois et al., 2010b; Viktorovitch et al., 2007, 2010). If the device is conveniently designed, the excitation of the Fano resonance can lead to a complete switch of the reflectivity from zero reflection (i.e. complete transmission) to total reflection. Hence, any change in the refractive index of PSi induced by the presence of target molecules will lead to a shift of the resonance and to an abrupt change of reflectivity, as shown in fig. 2b.

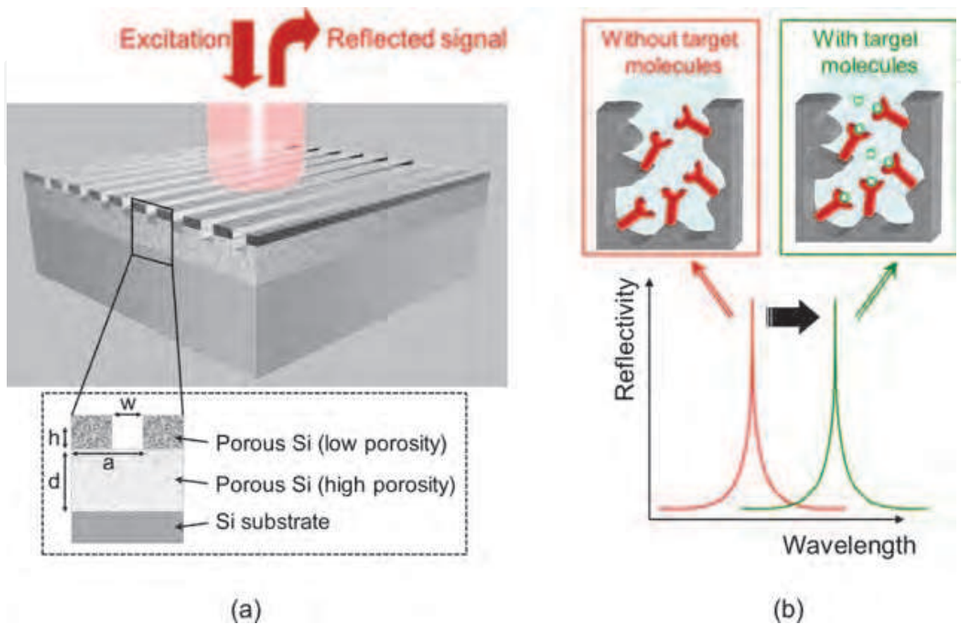

Fig. 2. Principle of the planar photonic crystal sensor: (a) device description, and (b) principle of optical sensing.

This type of biosensor presents the advantage to be used at normal incidence with relatively simple optical setups and no need for a prism. It can be directly integrated into an optical microchip in case multiple parallel sensing is desired. As will be discussed later in this chapter, its fabrication is easier than for the surface wave device, since only the top layer is patterned in this case.

The biosensor configuration presented in fig. 2 aims at monitoring reflection properties. This is the configuration that will be considered in the following sections. However, the same device could also be used in transmission, provided that it is reported onto a transparent substrate. Transmission configuration is particularly interesting when in-situ measurements are desired, as it prevents the incident beam from going through the analyte, which could lead to strong light absorption and sensitivity decrease. In-situ measurements could also be performed in reflection configuration if the design of the biosensor is carefully optimized in order to position the resonance in a wavelength range where the analyte absorption is low.

4. Experimental realization

The experimental realization of the PC-based biosensors requires several main steps. The first step is anodization of the substrate to form the PSi layers. It is the focus of section 4.1. Anodization is followed by lateral patterning of the PSi using standard nanolithography and dry etching techniques in order to fabricate the PC, as will be detailed in section 4.2. After

cleaning of the PSi devices to remove the remains from the patterning process, the PSi structure is slightly thermally oxidized (≤ 1 nm SiO_2) in order to enable subsequent silane-based functionalization. The details of PSi functionalization are discussed in section 4.3. In the following, we will consider the case of DNA sensing via hybridization of single-strand DNA targets with their complementary strands immobilized on the PSi surface. After immobilization of the DNA probes, the last required step is a capping to prevent non-specific absorption. The main steps in the biosensor realization are summarized again below:

anodization → patterning → oxidation → silanization → immobilization → capping → hybridization.

The influence of each step on the optical properties of the PSi is characterized by reflectivity measurements on 5 µm-thick PSi monolayers. After each step, the amounts of molecules infiltrated inside the pores can be quantitatively evaluated by fitting the reflectivity spectra with the refractive index models presented in section 5.1. The success of DNA immobilization and hybridization has also been verified by fluorescence measurements using probe and target molecules labelled with Cy3 and Cy5, respectively.

4.1 Porous silicon anodization

Anodization of silicon substrates to produce PSi is a well-described process in the literature. It takes place in hydrofluoric acid (HF) solution, where the silicon is dissolved by the fluorine ions thanks to the positive charges reaching the electrolyte/silicon interface (Kochergin & Föll, 2009; Lehmann & Gösele, 1991). Depending on substrate doping, current density and electrolyte concentration, the porosity and morphology of the fabricated PSi can be varied (Lehmann et al., 2000). In particular, PSi structures constituted of successive layers with different porosities, such as planar waveguides or multilayers, can be fabricated by controlled variation of the current density during anodization.

Fig. 3a shows a schematic view of the cell used to prepare our PSi samples. In order to fabricate meso-PSi, highly P-doped silicon substrates are used. The substrate is placed at the bottom of the anodization cell on a copper electrode, and in contact with the HF/H_2O/ethanol (35%/35%/30%) electrolyte. The second electrode made of platinum is immersed in the electrolyte at the top of the cell.

When preparing PSi layers for optical application, good care has to be taken that the roughness at the interfaces between the layers is low enough to prevent light scattering. Hence, anodization takes place at low temperature (-40°C) in order to enhance the viscosity of the electrolyte, which has been shown to strongly reduce interface roughness (Setzu et al., 1998). Working at low temperature also allows for a better control of the anodization velocities, thus for a better control of the layer thicknesses. Fig. 3b presents a scanning electron microscope (SEM) picture of a fabricated SW device consisting of PSi layers with alternative porosities of 80% and 35% and a small surface layer with 35% porosity. In spite of the roughness due to sample cleaving, very smooth interfaces between the layers can be seen. The surface layer has a well-controlled thickness as thin as 60 nm.

After fabrication, the PSi structures are systematically characterized by reflectivity measurements in the 900-1700 nm infra-red range, in order to check the porosity, layer thickness and homogeneity. Fits of the reflectivity spectra are performed using the refractive index models and the optical simulation methods presented in section 5.

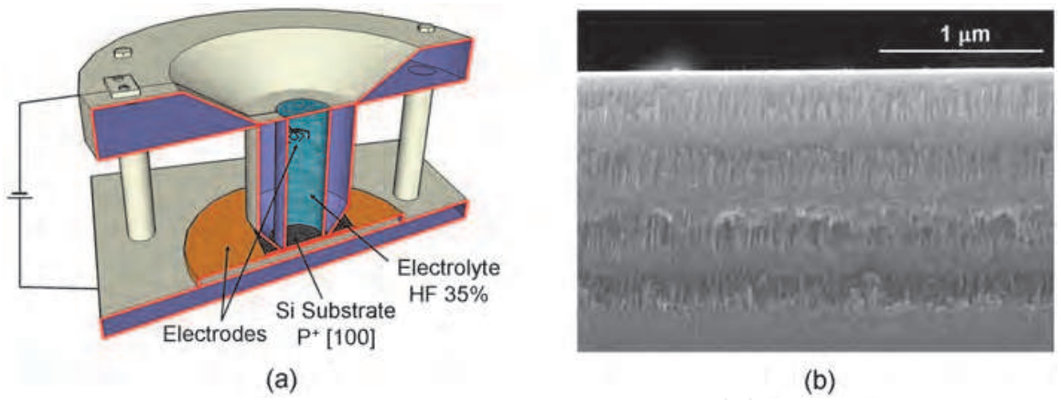

Fig. 3. (a) Schematic view of the anodization cell used to prepare the PSi samples, and (b) SEM picture showing an example of PSi multilayer.

4.2 Porous silicon patterning

After fabrication of the PSi layers, the next step in biosensor realization is PSi patterning to build the PC devices. The challenge here consists in deeply patterning a material that is itself nanostructured, anisotropic, and highly insulating, at a submicron scale. The desired air slits should have perfectly vertical walls, a typical width of 200 to 400 nm, a period below 1 µm, and an aspect ratio – i.e. depth/width ratio – of 2 to 4.

Different ways have been explored to obtain patterns in PSi at a submicron scale. Among them, photo-dissolution appears to be a promising technique, which uses holographic setups to create light patterns into the material and locally dissolve the material (Lerondel et al., 1997). Similarly, photo-oxidation has also been proposed as an alternative to locally oxidize and selectively etch patterns into PSi layers (Park et al., 2008).

Different nanoimprint techniques have also been proposed, such as soft lithography where PSi is put in contact with a polymer stamp and selectively detached from the substrate (Sirbuly et al., 2003). Very recently, patterning of PSi layers via nanoimprint using silicon stamps has been proposed (Ryckman et al., 2010). This technique allows for the realization of very well defined gratings; however, the PSi inside the patterns might get damaged. The pattern aspect ratio that can be reached using imprinting techniques is also quite limited.

In order to reach the desired depth required for our PC devices, a patterning process based on electron-beam lithography and reactive ion etching (RIE) has been selected. Very few reports on PSi patterning using dry etching techniques can be found in literature. The processes proposed are based on fluorine (Arens-Fischer et al., 2000; Tserepi et al., 2003) or chlorine plasmas (Meade & Sailor, 2007) and have been used to realize patterns with widths in the 10-100 µm range. In spite of these encouraging achievements, PSi patterning at sub-micrometer scale with high aspect ratios remains a real challenge for many reasons: the porous nanostructure of the material and its anisotropic morphology leading to poor efficiency in the case of such directional etching processes, the large internal surface of PSi favouring high sensitivity to contaminations such as polymer deposition during plasma etching, as well as the strongly insulating nature of the material.

The different steps in the realization of the PSi PCs are presented in fig. 4. After fabrication of the PSi by anodization, a silica layer is deposited by sputtering. This layer serves a triple purpose, since it helps homogenising the surface of the sample for subsequent resist spin-coating and lithography, it prevents the resist from penetrating into the material pores, and

it is used as a hard mask for RIE. After deposition of the silica layer, electron-beam lithography is carried out using PMMA A4 resist, and the resist patterns are transferred into the underlying silica layer by a CHF_3-based RIE process. The patterned silica layer is then used as a hard mask for PSi etching which occurs in SF_6/Ar plasma.

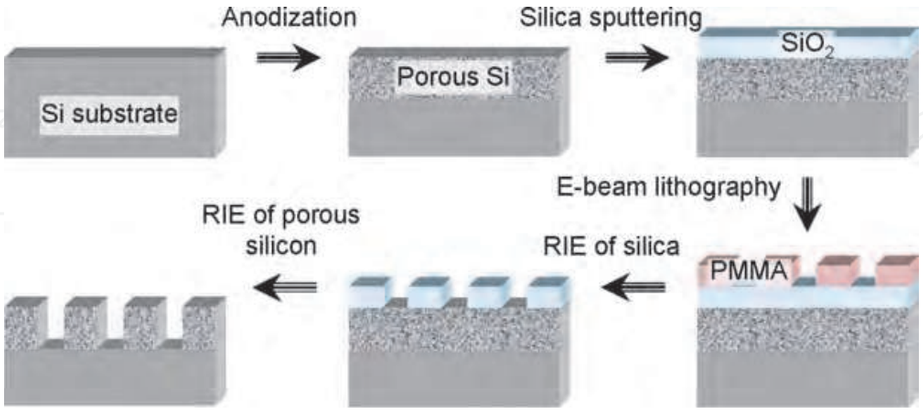

Fig. 4. The different steps of the patterning process used to realize PCs in PSi.

After careful optimization of each step of the PC realization process, in particular PSi patterning in SF_6-based RIE, deep trenches with vertical walls and aspect ratio of about 2 were successfully etched into the PSi. Fig. 5a shows an example of trenches realized in a PSi structure constituted of two layers with different porosity, 35% and 80% for the top and bottom layer, respectively. It can be observed that the RIE process enables to etch both porosities with perfectly vertical walls and no visible transition between the two layers in spite of their very different morphological and electrical properties.

The etching efficiency of the RIE process strongly decreases with increasing porosity. Hence, the pattern depth that can be reached is limited in the presence of 80% porosity layers, and the process presented above has to be adapted to allow for the devices fabrication.

In the case of planar PC fabrication where only the top layer with 35% porosity is patterned, the limitation in etching efficiency is induced by the presence of the underlying highly-insulating 80%porosity substrate. In order to reach deeper patterns, anodization of the high-porosity substrate can be performed after patterning of the top layer. Fig. 5b shows a SEM view of a fabricated planar PC device which consists of a 700 nm-thick PSi layer with 35% porosity on top of a substrate with 80% porosity. The width and period of the trenches are 400 nm and 900 nm, respectively. The high-porosity substrate was anodized after patterning of the top layer. A very smooth interface between the two porous layers can be observed.

In the case of the SW device, much deeper trenches are required, since at least 3 multilayer periods should be patterned. A well-known way to achieve deep etching is to use cyclic processes including passivation steps to provide both sidewall verticality and protection of the etching mask. However, such a process should be avoided in the case of PSi, as it would lead to strong polymerization inside the PSi pores that would harden considerably the material etching over time, as well as prohibit any subsequent biochemical functionalization. In order to reach the desired number of patterned multilayer periods, a new process using a more selective hard mask has to be developed. One way would be to consider metallic masks; however, the issue of metal contamination of the internal PSi surface exposed to the RIE environment has to be carefully investigated, as it may also influence subsequent biochemical functionalization.

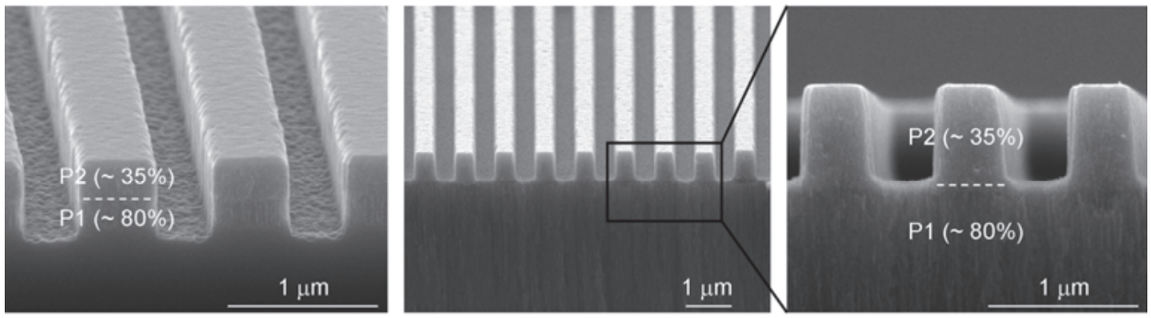

Fig. 5. (a) SEM image showing a preliminary result of patterning of PSi layers with different porosities P1 (80%) and P2 (35%). (b) SEM images of fabricated planar PC in PSi. The period of the patterns is 900 nm, and the device has a total size of 100 μm x 100 μm.

Another issue to tackle is the contamination of the PSi by fluorine during the RIE process. Indeed, the fluorine contained in the plasma can react with inevitable carbon contamination to form a fluorocarbon layer that deposits onto the PSi walls in the depth of the material. Special treatments are currently under development to clean the PSi walls from this contamination. Anodizing the substrate after RIE like in the case of the planar PC device is also a good way to avoid this contamination.

4.3 Porous silicon functionalization for DNA sensing

The bioselective element of biosensors is usually based on the immobilization of biomolecules on the surface of the transducer. The immobilization reaction can be achieved by physisorption through weak interactions (van der Waals, coulombic forces), by crosslinking with glutaraldehyde via an aminated surface (Rong et al., 2008) or SMCC via a thiolated surface, by entrapment or by chemisorption via covalent bonding.

Covalent immobilization reactions of biomolecules require chemical functionalization of the surface. These chemical groups can be introduced by plasma, polymer coatings… Hetero-cross linkers are also widely used. These molecules have two functional groups: one reacting with the material and one reacting with the biomolecules to be immobilized.

PSi has already been used as a large surface area matrix for immobilization of different kinds of biomolecules including enzymes (Drott et al., 1997), DNA fragments (De Stefano et al., 2007) and antibodies (Betty, 2009). Chemical functionalization of PSi can either involve the native Si-H terminated surfaces or the Si-O bond resulting from PSi oxidation.

Native Si-H surfaces can lead to Si-C or Si-Si bonds via organometallic reactions or via dehydrogenative silane coupling, respectively (Stewart & Buriak, 2000). The hydrosilylation reaction of alkyne and alkene with Si-H leads to the formation of Si-C bond with reduction of the C-C multiple bond. It proceeds with appreciable rate in the presence of white light, Lewis acid or by thermal activation. Similarly, formation of Si-C can be obtained by reaction of Grignard (Stewart & Buriak, 2000) or by electrografting reactions with organo halide (Gurtner et al., 1999) or alkyne (Robins et al., 1999). Si-C bonds can also be formed by cleavage of Si-Si linkage by reacting organolithium (Kim & Laibinis, 1998) or by electrochemical reduction of alkynes (Robins et al., 1999).

Oxidation of silicon results in the incorporation of oxygen, leading to a surface bearing terminal silanol groups. These groups can readily react with silazane, alkoxy silane or

organo silyl halide to form a siloxane bridge Si-O-Si. Organo silane can be mono or multifunctional (tri or di-chloro or -alkoxysilane). Multifunctional silane is usually preferred due to its higher reactivity and because it can lead to lower non-specific binding. Silanization with aminopropyl triethoxy silane or 3-glycidopropyl trimethoxy silane is well documented in the literature (Dugas et al., 2010a).

With multifunctional silane, additional intermolecular dehydration reactions between adjacent organo silanols lead to a 2D network. This polycondensation reaction needs to be perfectly monitored, otherwise it will lead to an anarchic 3D network and consequently to non-reproducible surface chemistry and obstruction of the PSi pores. An alternative solution is the use of monofunctional silane. Indeed, in this case each silane molecule can only react with the surface to form a siloxane bridge or with another silane molecule to form a dimer (Dugas et al., 2010b). The dimer is eliminated by subsequent washing. Therefore, no polymeric network is formed. The lower reactivity of monofunctional silane can be compensated by the use of silazane groups allowing for the complete reaction of all surface accessible silanols as demonstrated by Dugas (Dugas & Chevalier, 2003). The obtained layer was demonstrated to be reproducible and stable under harsh conditions.

Our process uses a monofunctional silane, *tert*-butyl-11-(dimethylamino)silylundecanoate which is an organo silazane bearing an ester function. Chemical functionalization of silica (Bras et al., 2004), PSi (Bessueille et al., 2005) and glass have been reported using this molecule from solution in pentane or from gas phase (Phaner-Goutorbe et al., 2011). As illustrated in fig. 6, after silanization, the *tert*-butyl ester is converted into the corresponding carboxylic acid by acidolysis in formic acid and activated with N-hydroxy succinimide. The obtained NHS ester surfaces can be employed for amine coupling. The resulting surface has a molecule density of $2x10^{14}$ molecules/cm². Immobilization of amino-modified oligonucleotide from diluted solution (25 µM) yielded to 3 – $4x10^{11}$ strands/cm². Hybridization yield with single stranded synthetic oligonucleotide is 10-20% (Dugas et al., 2004).

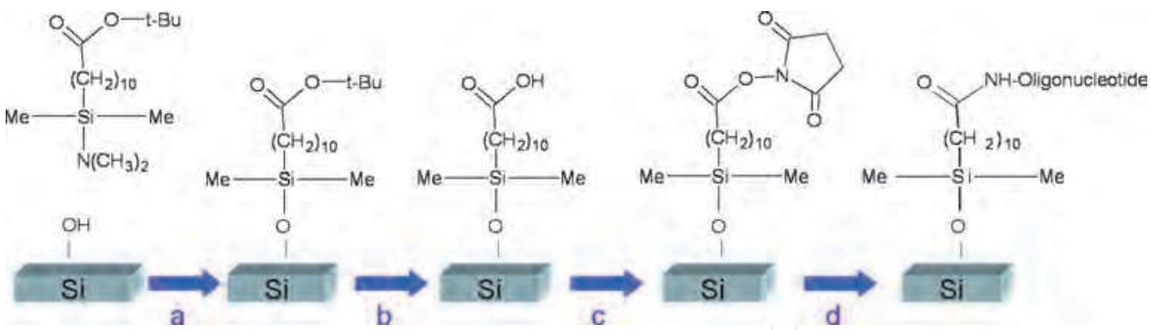

Fig. 6. Amino modified oligonucleotide are covalently immobilized by formation of an amide bond. After surface silanization with the monovalent silane uses *tert*-butyl-11-(dimethylamino)silylundecanoate (a), the *tert*-butyl ester group is removed leading to the corresponding carboxylic function (b). Activation (c) with diisoprpyl carbodiimide/ N-hydroxysuccinimide allows for the reaction with amino modified oliganucleotide (d) leading to the formation of an amide bond.

The resulting covalent immobilization of oligonucleotides can withstand 25 successive cycles of hybridization/denaturation (in 0.1 N NaOH) onto the same surface without observing any degradation, as well as deprotection/oxidation steps performed during

phosphoramidite oligonucleotide synthesis (Bessueille et al., 2005; Cloarec et al., 2008). Immobilization of peptides (Soultani-Vigneron et al., 2005), histones (El Khoury et al., 2010) or carbohydrates (Chevolot et al., 2007; Moni et al., 2009; Zhang et al., 2009) has also been achieved.

5. Modeling of optical properties

Modelling of PSi based PCs includes two different aspects: the calculation of the refractive index, and the simulation of the optical properties. They are presented in the following.

5.1 Calculation of porous silicon refractive index

PSi is a composite medium with a pore size much smaller than the wavelength of light. Hence, the dielectric response can be described through an effective dielectric function. A complete review of the different isotropic and anisotropic models used for the calculation of PSi refractive index has recently been published (Kochergin & Föll, 2009). In the isotropic approximation, the main models used for the calculation of the effective dielectric function are the Bruggeman and Landau Lifshitz Looyenga (LLL) effective medium approximations (EMA) that can be defined by the following expressions (Bruggeman, 1935; Looyenga, 1965):

$$Bruggeman: \sum_i f_i \frac{\varepsilon_i - \varepsilon_{eff}}{\varepsilon_i + 2\varepsilon_{eff}} = 0 \qquad LLL: \ \varepsilon_{eff} = \left(\sum_i \left(\varepsilon_i^{1/3} - \varepsilon_{Si}^{1/3} \right) f_i + \varepsilon_{Si}^{1/3} \right)^3 , \ \sum_i f_i = 1 \qquad (1)$$

where f_i and ε_i are the volume fraction and the complex dielectric function of material i, respectively. The refractive index of materials is related to the permittivity ε with $\varepsilon = n^2$. The refractive indices of Si and SiO_2 can be obtained from the Palik handbook (Palik, 1998). As the materials are used in their transparency domain, the variations of their refractive indices with the wavelength are deduced from a Cauchy law, using the parameters given in table 1:

$n = A + \frac{B}{\lambda^2} + \frac{C}{\lambda^4}$		A	B	C
	Si	3.4227	0.1104	0.041
	SiO_2	1.4213	0.0856	-0.0735

Table 1. Cauchy law and values of the Cauchy coefficients used for the modelling.

In order to consider absorption of light in the doped silicon substrate, variations of the refractive index induced by free carriers absorption have to be taken into account. The relation proposed by Soref is used (Soref & Bennett, 1987), which requires calculation of the electron and holes mobilities depending on substrate doping (Sedra & Smith, 1997).

The models presented above have been implemented to fit experimental data, in particular the reflectivity measurements performed on PSi layers. As an example, the reflectivity spectra of a PSi monolayer before and after an oxidation step are plotted on fig. 7. The parameters of the Bruggeman and LLL models and the thickness of the PSi monolayer are obtained using a Levenberg Marquardt nonlinear fitting method (Press et al., 1992). The results obtained using the Bruggeman and LLL models reproduce well the experimental indices deduced from reflectivity measurements. For this particular sample, the PSi layer was found to have an initial porosity of 70% and 73%, respectively, and a thickness of 4.735 and 4.741 µm, respectively, for the Bruggeman and LLL models. Both models gave a silica

fraction of 11% after oxidation. Hence, the fitted parameters are very close for both models, with a relative variation below 5%.

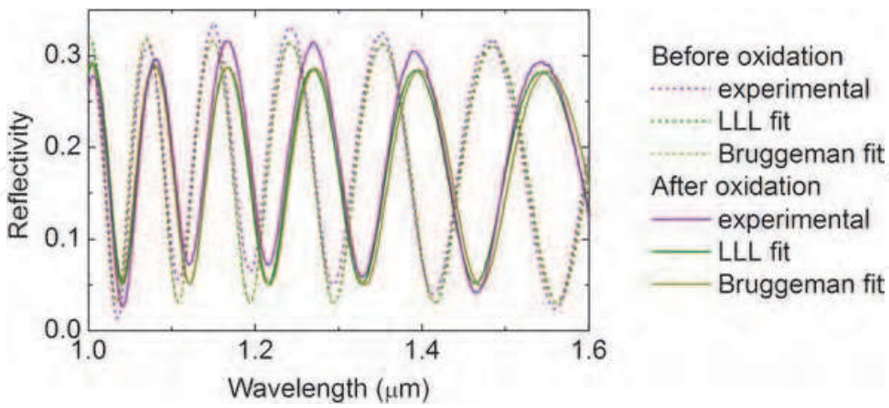

Fig. 7. Evolution of the reflectivity of a PSi monolayer before (dash) and after (straight) oxidation step. The experimental data has been fitted with the Bruggeman and LLL models.

In the following sections, the refractive indices will be determined using the LLL model. Fitting all experimental data using the LLL model, we could evaluate that the volume fractions of silica after oxidation correspond to the formation of a layer having a thickness of 1 nm on the internal PSi walls, for both porosities considered (35% and 80%). This is consistent with the experimental calibrations of the oxidation process. Similarly, the volume fractions of silane molecules deduced from the experimental spectra after silanization are equivalent to the formation of dense layers with refractive index 1.4 and thickness around 1.7 nm covering the internal PSi walls. This layer thickness is similar for both porosities and consistent with the developed length of the silane molecules used (~ 1.7 nm).

5.1 Simulation of optical properties

Numerical modelling is a major concern for the study of PC structures. Along the years, two main approaches have emerged: the plane wave expansion (PWE) and the finite difference in the time domain (FDTD) method.

The PWE method relies on the translation symmetry of the PC structure. The method assumes a time harmonic evolution of the electromagnetic fields. In this case, the Maxwell equations lead to the following general Helmoltz equation:

$$\vec{\nabla}\times\left(\frac{1}{\varepsilon_r(\vec{r})}\vec{\nabla}\times\vec{H}(\vec{r})\right)=\left(\frac{\omega}{c}\right)^2\vec{H}(\vec{r}) \tag{2}$$

where $\boldsymbol{H}$ stands for the magnetic field, ω the pulsation and ε_r is the relative dielectric permittivity.

This is an eigenvalue problem, which can be solved using a Fourier expansion along the vectors of the reciprocal lattice. It leads to the dispersion relation $\omega = \omega(\boldsymbol{k})$ where $\boldsymbol{k}(k_x,k_y,k_z)$ is the light wave vector. This approach enables a very efficient calculation of the band diagram, giving information on photonic band gaps, group and phase velocity… of the infinite periodic structure. However, this useful approach suffers from some limitations. In its common formulation, it could not easily handle losses (lossy material, leaky modes…). In

the following sections, a free software package is used, MIT Photonic Bands (MPB) (Johnson & Joannopoulos, 2001).
When it comes to real finite devices, the FDTD method is more suited. This method relies on the discretization in time and space of the Maxwell equations (Taflove & Hagness, 2005):

$$\frac{\partial \vec{E}}{\partial t} = \frac{1}{\varepsilon} \nabla \times \vec{H} \quad and \quad \frac{\partial \vec{H}}{\partial t} = -\frac{1}{\mu} \nabla \times \vec{E} \tag{3}$$

where $\boldsymbol{E}$ and $\boldsymbol{H}$ stand for the electric and magnetic field, respectively, and ε and μ for the dielectric and magnetic permittivity, respectively.
The numerical experiments generally consist in sending an electromagnetic pulse onto the structure and to monitor its response with time. A single simulation run is necessary to get the frequency response thanks to the Fourier transform of the time response. It gives access to the spectral response of the system (transmission, reflection). The ability of FDTD to solve open problems is very useful for the study of microcavities and leaky modes. It gives access to the quality factor (Q factor = $\lambda/\Delta\lambda$) of resonances. Moreover, an electromagnetic field map at a given frequency could be easily obtained thanks to the discrete Fourier transform. As this method has achieved its full maturity, it can handle dispersive and lossy materials, non-uniform mesh, non-linear effects… Another interesting development is the implementation of periodic boundary conditions which enable the study of infinite PCs. Compared to the PWE, the FDTD method is less efficient; however, it allows for the study of leaky modes (modes above the light line, i.e. in the free-state continuum). The FDTD method also requires a lot of computing resources which are now available, thanks to ever evolving microprocessor power, and it can be by nature easily parallelized.

6. Performance study of photonic-crystal-based biosensors

In this section, a performance study of the two PC-based biosensors is discussed, using the tools and methods presented above. Both devices are considered for use in the infra-red range at around 1300-1500 nm wavelength where absorption losses in the material can be neglected. In this case, the main source of losses in PSi devices is expected to be scattering at the interface of the silicon nanocrystallites (Ferrand & Romestain, 2000). Experimental measurements show that the losses are only a few cm^{-1} in this wavelength range and should not alter significantly the sensor response. Therefore, we expect our theoretical predictions to be in good agreement with experimental results.

6.1 Surface-wave biosensor

The very high sensitivity of the SW sensor in the 1D – i.e., unpatterned – configuration has been demonstrated both theoretically and experimentally. In particular, we have observed angular variations as large as 20° after grafting of amine molecules inside the PSi device (Guillermain et al., 2007). In further studies, much smaller amounts of biomolecules were considered, in order to evaluate the limit of detection of the biosensor. It was demonstrated that convenient lateral patterning could enhance the sensitivity of the biosensor by an order of magnitude (Jamois et al., 2010a). In these previous studies, we focussed on SW sensors having a high-index surface layer with porosity 35%. Such porosity enables to reach very high sensitivities due to very large PSi internal surface. However, due to the small pore size (< 10 nm) sensing is limited to small biomolecules. In the following, we consider the case of

SW sensors having a surface layer with larger porosity 55%, which might yield a slightly lower sensitivity due to smaller PSi internal surface, but enables sensing of larger molecules. The devices consist of a multilayer with period a and standard porosities P1 = 80% and P2 = 35%, respectively, with corresponding refractive indices n1 = 1.4 and n2 = 2.5 deduced from the LLL model. The multilayer is terminated by a surface layer with porosity P_{surf} = 55% and refractive index 2.0. Fig. 8 shows the band diagram of the 1D PC for the propagation direction parallel to the surface. As the 1D PC is homogeneous in the direction of propagation, the bands of the 1D structure shown in fig. 8 are continuous. However, the continuity of the bands can be broken by introducing a periodic perturbation. If a periodic pattern is introduced in the direction of propagation, bands are back-folded at the edge of the lateral Brillouin zone – for wave vectors $k = \pi/a$ – resulting in local band flattening, i.e., a strong decrease of light velocity. After careful optimization of both the multilayer and the array of air slits, a 2D structure was obtained with a PBG large enough to assure a good confinement of the SW. The optimized parameters of the resulting 2D PC are thicknesses d1 = d2 = 0.5a for the multilayer, and w = 0.8a and a' = 1.2a for the width and period of the air slits, respectively. For a good comparison of the sensor performances, the layer thicknesses are the same for the 1D sensor as for the 2D device. Because the surface mode position within the PBG is highly sensitive to the thickness of the surface layer (Guillermain et al., 2006), optimization of the surface layer thickness has also been necessary to position the SW in the middle of the PBG and thus provide a good light confinement within the surface layer. The optimized thickness of the surface layer is h = 0.4a for both 1D and 2D devices. Fig. 8 shows the band structures for the optimized 1D and 2D SW devices.

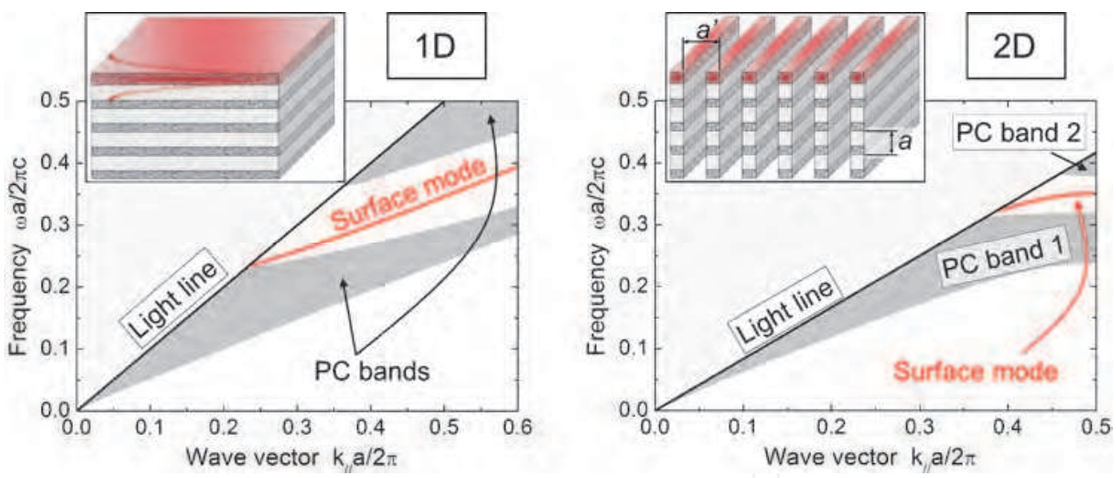

Fig. 8. Simulated band structures (MPB) of the SW sensor in air environment for the unpatterned (1D) and patterned (2D) configurations.

As plane-wave simulations consider a semi-infinite structure that is not experimentally achievable, periodic FDTD simulations were also performed to evaluate the performances of more realistic devices. Considering a multilayer consisting of 6 periods and varying the depth of the air slits, it could be verified that the optical properties of the device do not vary significantly with an increase of the slits depth, provided that the air slits are at least 3 multilayer periods deep. Hence, our band structure calculations can well describe the expected device performances, if the depth of the patterns in the experimental 2D sensor reaches 3 multilayer periods.

In order to demonstrate the high device sensitivity, a comparative study of the optical response in the 1D and the 2D cases has been performed in air environment, considering as an initial state a slightly oxidized porous structure (~ 1 nm SiO_2) and varying the amount of molecules grafted onto the pore walls. Note that similar results would be obtained in the case of specific biomolecular recognition, provided that the initial refractive index of PSi is adjusted to take into account biochemical functionalization. Moreover, we consider the limiting case where molecule grafting is restricted to the surface layer in order to take into account the inhomogeneous infiltration of liquids and biomolecules inside meso-PSi, which is the largest close to the surface and decreases in the depth of the multilayer, as was demonstrated using labelled proteins (De Stefano & D'Auria, 2007). We should point out that this restriction is underestimating the response of the biosensors.
The shift in the band structure induced by the grafting of 2.5%biomolecules inside the PSi is presented in fig. 9 for both 1D and 2D devices. It can be seen that the much flatter surface band of the 2D sensor leads to much larger variations in wave vector and in resulting coupling angle. In the presence of the biomolecules, the shift in coupling angle is 0.7° for the unpatterned device and as large as 4.0° for the patterned sensor. This corresponds to an increase in sensitivity of the 2D device by a factor 6 compared to the 1D case.

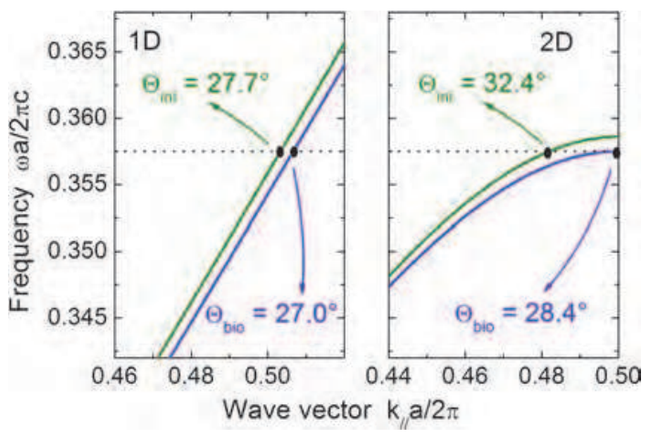

Fig. 9. Optical response of the surface wave sensor to the grafting of 2.5% biomolecules in air environment for the unpatterned (1D) and patterned (2D) configurations.

The variation in coupling angle and in refractive index depending on the amount of biomolecules is presented in fig. 10 for the 2D biosensor. For a better understanding of the amount of biomolecules infiltrated inside the pores, it is also expressed as the equivalent thickness d_{bio} of a dense monolayer having the same volume and homogeneously coating the internal surface of the pores. This formalism has already been used in other studies of photonic sensors based on PSi, and has proven to yield good agreement between theoretical predictions and experimental results (Ouyang et al., 2006). As can be seen in fig. 10a, a variation in coupling angle as large as 13.5° is expected for the grafting of a dense monolayer of biomolecules with thickness 1.7, which corresponds to the case of our silanization process. A much smaller amount of molecules of 0.1% – equivalent to a dense layer with thickness 0.01 nm – would still induce a variation in coupling angle of 1°, with a corresponding variation in refractive index of $6x10^{-4}$. Considering that high-performance SPR setups can detect angular variations as small as 0.001°, we can conclude that the limit of detection of the SW sensor is very low.

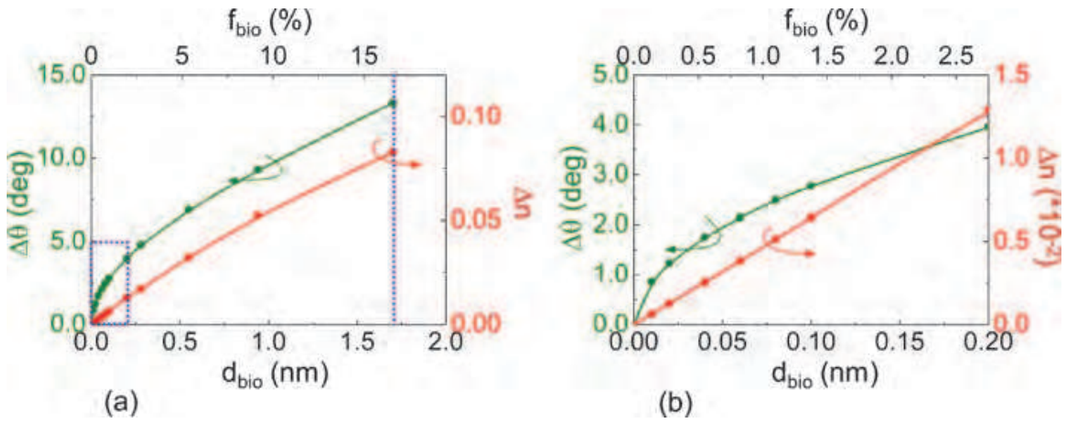

Fig. 10. Simulated optical response (MPB) of the SW sensor in air environment as a function of the amount of detected biomolecules: (a) for large amounts, and (b) for smaller amounts. The optical response is expressed both as a shift in coupling angle (Δθ) and as the corresponding refractive index variation in the top layer (Δn). The amount of biomolecules is given as a volume fraction inside the PSi (f_{bio}) and as an equivalent thickness (d_{bio}). The blue dashed line indicates the expected device response to silane grafting.

6.2 Planar photonic-crystal biosensor

The optical response of the planar PC observed at normal incidence shows the superposition between interferences occurring inside the PSi layers and the excited Fano resonances. In order to maximize the variation of reflection induced by biosensing events, the structure has to be optimized to position the resonance in a zero of reflectivity corresponding to destructive interferences within the PSi layers. This way, the reflected signal at resonance can be switched between 0% and 100%. The device optimization was performed combining plane-wave and FDTD simulations for the TE polarization where the electric field is parallel to the slits (Jamois et al., 2010b). After optimization, the band structure presented in fig. 11a was obtained, yielding a Fano resonance with very sharp features at a relative frequency $a/\lambda = 0.66$ very close to the Γ point, where it can be excited at normal incidence. The Q factor of the resonance can be as high as 1200 for the optimized 1D PC with top layer thickness $h = 0.75a$ and trench width $w = 0.4a$. Note that the Q factor is very sensitive to the thickness of the top PSi layer: increasing or decreasing the thickness by only 50 nm results in a reduction of the Q factor by several hundred. As our fabrication process enables a very good control of the layer thicknesses, the sensitivity of the Q factor should not have a significant impact on the device performances. The Q factor also strongly varies with the filling factor, i.e., the relative width of the air slits, which means that the experimental fabrication process should be carefully calibrated to obtain the desired slit widths.

In order to evaluate the performance of the device for biosensing, a similar study was performed as in the case of the SW sensor, considering as an initial state a slightly oxidized porous structure (~ 1 nm SiO_2) and varying the amount of molecules grafted onto the pore walls. Fig. 11b shows the shift of the resonance depending on the amount of biomolecules. Due to the finesse of the resonance, the presence of only 0.35% biomolecules leads to a shift of the resonance large enough to induce a dramatic decrease in reflectivity from 100% (green curve) down to 32% (red curve). The wavelength variation of the resonance depending on the amount of biomolecules is presented in fig. 12a-b, where the amount of biomolecules is

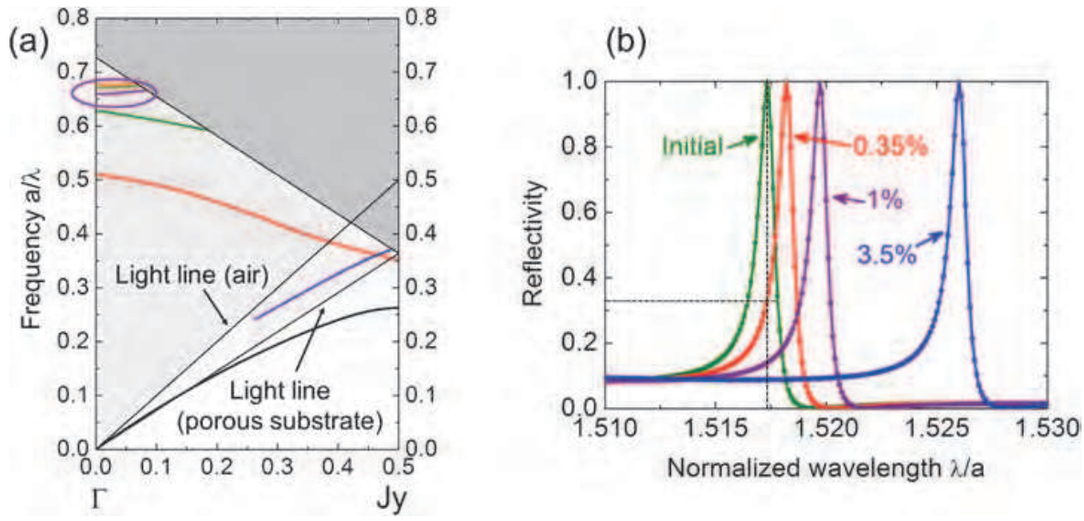

Fig. 11. (a) Band structure of the planar photonic crystal device (MPB simulation). The resonance of interest for biosensing is marked by a purple circle. (b) Reflectivity behaviour showing the resonance shift depending on the amount of biomolecules (FDTD simulation).

again expressed both as a volume fraction f_{bio} and as an equivalent thickness d_{bio}. The corresponding refractive index variation of the top PSi layer is also shown. As this study is performed in air environment, the wavelength variation is determined for an initial resonance centred at 1500 nm. Fig. 12a highlights the very large sensitivity of the device; indeed, in the case of grafting of a dense monolayer of silane molecules with a length of 1.7 nm, the expected shift of the resonance is larger than 50 nm. Fig. 12b demonstrates that smaller amounts of biomolecules can be well detected as well, since the grafting of 0.35% of molecules – equivalent to a dense monolayer with only 0.02 nm thickness – would induce a wavelength shift larger than 1 nm, which is in good agreement with fig. 11b. The induced refractive index variation for this small amount of biomolecules would be below $2x10^{-3}$.

In order to evaluate the performances of the sensor for in-situ measurements, the same study has been performed in aqueous environment. In this case, all the pores of the PSi layers as well as the trenches are completely filled with water. The presence of water inside the pores induces an increase of the oxidized PSi refractive index to 2.52 and 1.63, respectively, for the top layer and the substrate. Hence, the index contrasts remain quite large between the layers of different porosities, as well as between the PSi and the water-filled slits. After a new optimization of the photonic crystal to take into account the new index configuration, a similar Fano resonance was found to yield a Q factor above 1000 if the thickness of the top layer is adjusted to $0.8a$. This means that the presence of water does not dramatically alter the device performances. Fig. 12c-d shows the optical response of the sensor in aqueous environment with varying amount of biomolecules. For a better comparison with the results obtained in air environment, the wavelength shifts have been calculated for a resonance centred at 1500 nm. When using the device at shorter wavelength (e.g., at 1300 nm where water absorption is strongly reduced) the wavelength shift of the resonance is correspondingly slightly smaller. Due to the lower refractive index difference between biomolecules and water ($\Delta n < 0.1$) than between biomolecules and air ($\Delta n \sim 1.4$), it is expected that the same volume of molecules induces a lower optical response in aqueous environment. In this case, silane grafting shown in fig. 12c would induce a shift of the

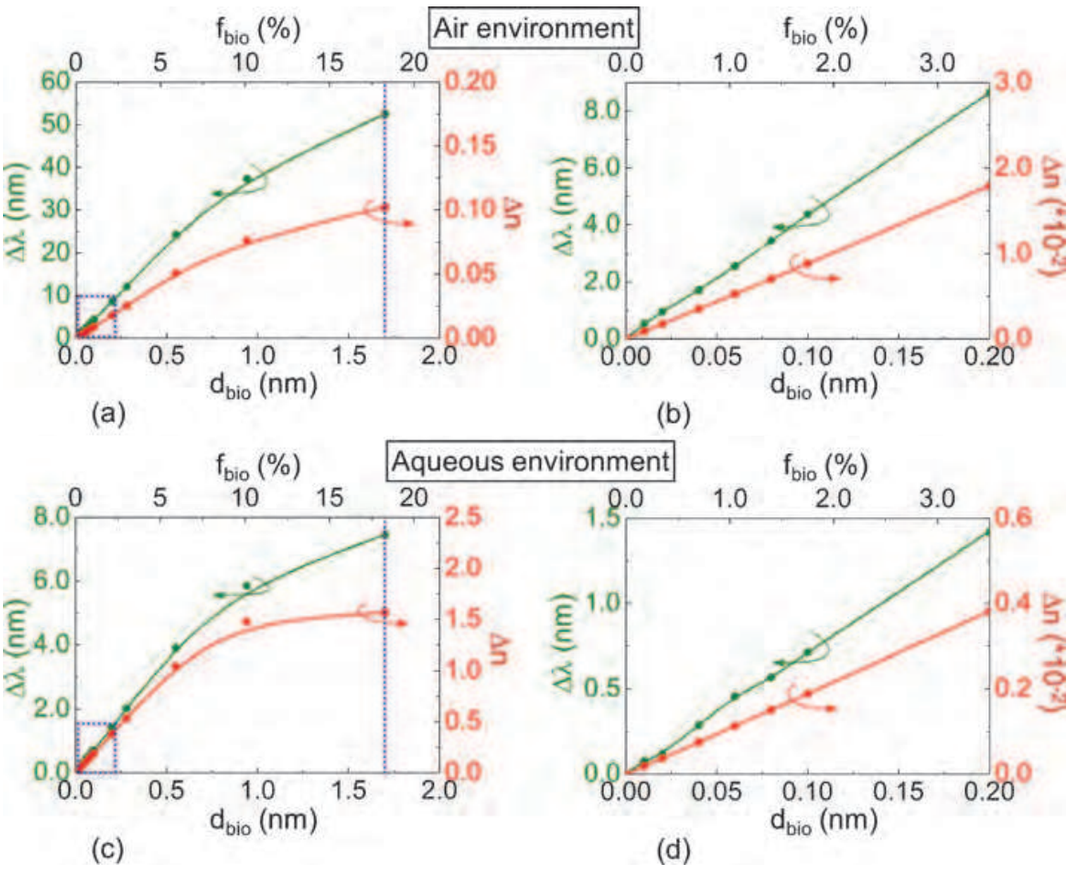

Fig. 12. Simulated optical response (MPB) of the planar photonic crystal biosensor in air and aqueous environment, respectively: (a), (c) for large amounts of biomolecules, and (b), (d) for smaller amounts. The optical response is expressed both in wavelength shift (Δλ) and in corresponding refractive index variation in the top layer (Δn). The amount of biomolecules is given as a volume fraction (f_{bio}) and as an equivalent thickness (d_{bio}). The blue dashed line indicates the expected device response to silane grafting.

resonance by 7.5 nm, which corresponds to a decrease in sensitivity by a factor 7 compared to the sensor in air environment. However, we can see in fig. 12d that very small amounts of biomolecules can still be detected, as the grafting of 1% of biomolecules, equivalent to a dense monolayer with 0.06 nm thickness, would induce a wavelength shift of 0.5 nm.

In order to study the experimental response of the biosensor, the process discussed in section 4 was used to realize devices similar to the one shown in fig 5b. The fabricated devices were then functionalized and their optical properties were characterized by reflectivity measurements at each main functionalization step. The optical setup used for the reflectivity measurements, presented in fig. 13a, is equipped with a wide band 1200-1600 nm laser diode source and an InGaAs detector. Light is focussed on the 100 µm x 100 µm size device via a microscope objective. Nano-positioning of the sample is achieved via an XYZ piezoelectric table and is monitored with a visualization camera.

The optical response of the device is presented in fig. 13b. The green spectrum shows the reflectivity of the device after oxidation. The oscillations in reflectivity due to the interferences in the PSi substrate are clearly visible. Superimposed to these oscillations, 2

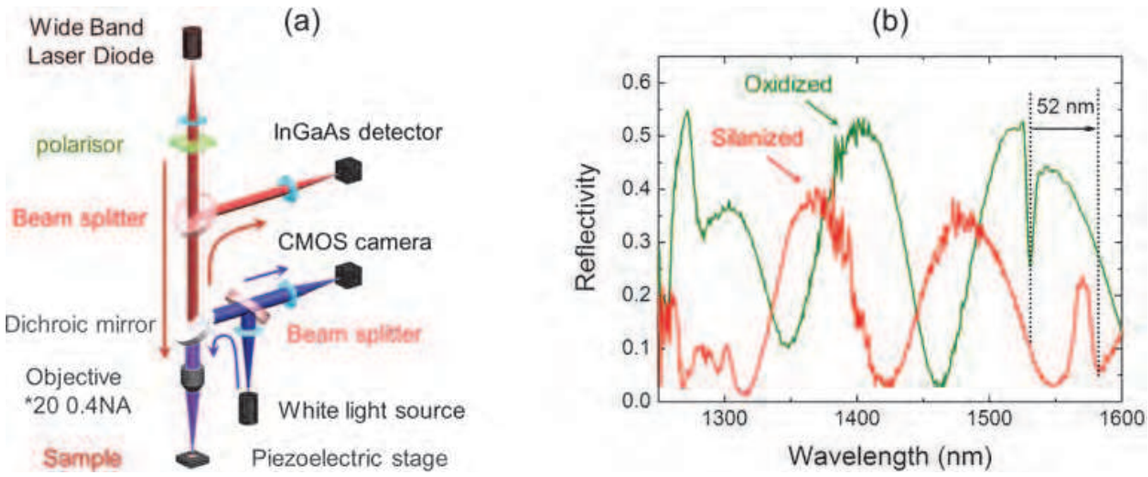

Fig. 13. (a) Schematic view of the optical setup. (b) Reflectivity measurements of the planar PC device, after oxidation (green curve) and after subsequent silanization (red curve).

main resonances can be seen, the first one around 1280 nm and a sharper resonance at 1530 nm. This second resonance is the Fano resonance of interest for biosensing. After silanization, the same device has been characterized again and the red spectrum has been obtained. Comparing the two spectra, it can be observed that the interference fringes have shifted, indicating a change in refractive index of the PSi layer and successful silane grafting. Moreover, the second resonance that was initially at 1530 nm shows a strong 52 nm red shift, which is in perfect agreement with the simulated expectations discussed in fig. 12.
After immobilization of DNA probes on the silanized PSi surface, the devices show strong 20 nm blue shifts, which are a signature of PSi corrosion due to remaining Si-H bonds (Steinem et al., 2004). Although the amount of Si-H and Si-OH bonds is very low – almost invisible on FTIR spectra – their presence is sufficient to induce a damage of the PSi structure with the resulting blue shift, and to prevent any quantitative measurement of the immobilized DNA molecules. Hence, both our oxidation process and the surface capping by the silane molecules should be further improved to completely eliminate the Si-H bonds or to prevent access from the water molecules to these H-bonds.

7. Conclusion

In this chapter, new concepts for meso-PSi integrated optical biosensors based on photonic crystals have been presented, as well as the study of their performances.
The first biosensor is based on the excitation of SW at the surface of a PC device. Such devices yield very high sensitivity that can be further enhanced by the introduction of lateral patterning. We demonstrated a gain in sensitivity by a factor 6 between the 1D and 2D biosensors. Another great property of this biosensor is the possibility to adjust the porosity of the surface layer depending on the size of the target biomolecules. One disadvantage of the SW device is that prism coupling requires large optical setups that are not convenient for mass applications. It also requires large device areas and is not compatible with on-chip multiple parallel sensing. These limitations can be overcome if the prism is replaced, e.g., by a grating and if a detection principle similar to SPRI setups is used. The other limitation of the SW sensor in its 2D configuration is a quite challenging technological realization due to

the depth of the slits that have to be patterned into the PSi multilayer. New processes are currently been developed to enable the fabrication and experimental study of these sensors.
The second biosensor is based on the excitation of Fano resonances in planar PCs at normal incidence. Such devices require simpler optical setups, they are very compact and can be directly integrated into optical microchips, enabling for multiple parallel sensing. They yield high sensitivity and their experimental realization is less challenging than in the case of SW devices. We demonstrated perfect agreement between the theoretical and experimental performances and shift of the resonance wavelength as large as 52 nm after grafting of a silane monolayer. Because the porosity of the top layer cannot be too large in order to yield good optical properties, these sensors are restricted to the detection of small biomolecules. Further optimization of the sensor design will help to overcome this limitation.
Therefore, PCs in PSi are a very promising route to realize high performance biosensors that can be fully integrated into optical microchips and used for in-situ analysis. As both the experimental realization and the theoretical design of the devices are still at the focus of intensive research, new exciting developments will certainly occur in a near future.

8. Acknowledgments

The experimental work is performed at the technological platform Nanolyon. R. Mazurczyk, P. Crémillieu, C. Seassal, A. Sabac and J.-L. Leclercq are kindly acknowledged for fruitful discussions on fabrication techniques and technical support. We are also very grateful to C. Martinet, G. Grenet, C. Botella, N. Blanchard, P. Regreny and D. Leonard for their help on physico-chemical characterization of PSi.
Financial support by the French ANR in the framework of the research project BiP BiP (JC09_440814), and the INSA-Lyon in the framework of a BQR project, as well as the CSC for PhD stipend funding are acknowledged.

9. References

Arens-Fischer, R.; Krüger, M.; Thönissen, M.; Ganse, V.; Hunkel, D.; Marso, M. & Lüth, H. (2000). Formation of porous silicon filter structures with different properties on small areas. *Journal of Porous Materials*, Vol. 7, pp. 223–225, ISSN 1380-2224

Bergveld, P. (1970). Development of an ion-sensitive solid state device for neurophysiological measurements, *IEEE Transactions on Biomedical Engineering* Vol. 17, pp. 70–71

Bessueille, F.; Dugas, V.; Vikulov, V.; Cloarec, J.-P.; Souteyrand, E. & Martin, J.R. (2005). Assessment of PSi substrate for well-characterised sensitive DNA chip implement. *Biosensors & Bioelectronics,* Vol. 21, No. 6, pp. 908-916, ISSN 01694332

Betty, C.A. (2009). Highly sensitive capacitive immunosensor based on PSi-polyaniline structure: Bias dependence on specificity. *Biosensors and Bioelectronics,* Vol. 25, No. 2, pp. 338-343, ISSN 0956-5663

Bonanno, L.M. & DeLouise, L.A. (2007). Whole blood optical sensor. *Biosensors & Bioelectronics,* Vol. 23, No. 3, pp. 444-448, ISSN 0956-5663

Bras, M.; Dugas, V.; Bessueille, F.; Cloarec, J.-P.; Martin, J.R.; Cabrera, M.; Chauvet, J.-P.; Souteyard, E. & Garrigues, M. (2004). Optimisation of a silicon/silicon dioxide substrate for a fluorescence DNA microarray. *Biosensors and Bioelectronics,* Vol. 20, No. 4, pp. 797-806, ISSN 09565663

Bruggeman, D.A.G. (1935). Berechnung Verschiedener Physikalischer Konstanten von Heterogenen Substanzen. *Annalen der Physik*, Vol. 24, pp. 636-664

Canham, L.T. (1990). Silicon quantum wire array fabrication by electrochemical and chemical dissolution of wafers. *Applied Physics Letters,* Vol. 57, No. 10, pp. 1046-1048, ISSN 0003-6951

Caras, S. & Janata, J. (1980). Field effect transistor sensitive to penicillin. *Analytical Chemistry*, Vol. 52, No. 12, pp. 1935-1937, ISSN 0003-2700

Chapron, J.; Alekseev, S.A.; Lysenko, V.; Zaitsev, V.N. & Barbier, D. (2007). Analysis of interaction between chemical agents and porous Si nanostructures using optical sensing properties of infra-red Rugate filters. *Sensors and Actuators B,* Vol. 120, No. 2, pp. 706-711, ISSN 0925-4005

Chevolot, Y.; Bouillon, C.; Vidal, S.; Morvan, F.; Meyer, A.; Cloarec, J.-P.; Jochum, A.; Praly, J.-P.; Vasseur, J.-J. & Souteyrand, E. (2007). DNA-Based Carbohydrate Biochips: A Platform for Surface Glyco-Engineering. *Angewandte Chemie-International Edition,* Vol. 46, No. 14, pp. 2398-2402, ISSN 1433-7851

Cloarec, J.-P.; Chevolot, Y.; Laurenceau, E.; Phaner-Goutorbe, M. & Souteyrand, E. (2008). A multidisciplinary approach for molecular diagnostics based on biosensors and microarrays. *IRBM,* Vol. 29, No. 2-3, pp. 105-127, ISSN 12979562

Cunin, F.; Schmedake, T. A.; Link, J.R.; Li, Y.Y.; Koh, J.; Bhatia, S.N. & Sailor, M.J. (2002). Biomolecular screening with encoded porous-silicon photonic crystals. *Nature Materials*, Vol. 1, No.1, pp. 39-41, ISSN 1476-1122

De Stefano, L.; Arcari, P.; Lamberti, A.; Sanges, C.; Rotiroti, L.; Rea, I. & Rendina, I. (2007). DNA Optical Detection Based on PSi Technology: from Biosensors to Biochips. *Sensors,* Vol. 7, No. 2, pp. 214-221, ISSN 1424-8220

De Stefano, L. & D'Auria, S. (2007). Confocal imaging of protein distributions in PSi optical structures. *Journal of Physics: Condensed Matter*, Vol. 19, pp. 395009, ISSN 0953-8984

Drott, J.; Lindstrom, K.; Rosengren, L. & Laurell, T. (1997). PSi as the carrier matrix in microstructured enzyme reactors yielding high enzyme activities. *Journal of Micromechanics and Microengineering,* Vol. 7, No. 1, pp. 14-23, ISSN 0960-1317

Dugas, V. & Chevalier, Y. (2003). Surface hydroxylation and silane grafting on fumed and thermal silica. *Journal of Colloid and Interface Science,* Vol. 264, No. 2, pp. 354-361, ISSN 00219797

Dugas, V.; Depret, G.; Chevalier, B.; Nesme, X. & Souteyrand, E. (2004). Immobilization of single-stranded DNA fragments to solid surfaces and their repeatable specific hybridization: covalent binding or adsorption? *Sensors and Actuators, B: Chemical,* Vol. 101, No. 1-2, pp. 112-121, ISSN 0925-4005

Dugas, V.; Elaissari, A. & Chevalier, Y. (2010a). *Surface Sensitization Techniques and Recognition Receptors Immobilization on Biosensors and Microarrays,* Recognition Receptors in Biosensors, M. Zourob, Springer Verlag, pp. 47-134, ISBN 978-1-4419-0918-3, New York (USA)

Dugas, V.; Demesmay, C.; Chevolot, Y. & Souteyrand, E. (2010b). *Use of Organosilanes in Biosensors*, Biotechnology in Agriculture, Industry and Medecine, Nova Science Publishers, Inc., ISBN 978-1-61668-029-9, New York (USA)

El Khoury, G.; Laurenceau, E.; Chevolot, Y.; Merieux, Y.; Desbos, A.; Fabien, N.; Rigal, D.; Souteyrand, E. & Cloarec, J.-P. (2010a). Development of miniaturized immunoassay: Influence of surface chemistry and comparison with enzyme-linked

immunosorbent assay and Western blot. *Analytical Biochemistry,* Vol. 400, No. 1, pp. 10-18, ISSN 0003-2697

Fan, X.; White, I.M.; Shopova, S.I.; Zhu, H.; Suter, J.D. & Sun, Y. (2008). Sensitive optical biosensors for unlabeled targets: A review. *Analytica Chimica Acta*, Vol. 620, pp. 8-26

Ferrand, P. & Romestain, R. (2000). Optical losses in PSi waveguides in the near-infrared: Effects of scattering. *Applied Physics Letters*, Vol. 77, pp. 3535-3537, ISSN 0003-6951

Guillermain, E.; Lysenko, V. & Benyattou, T. (2006). Surface wave photonic device based on PSi multilayers. *Journal of Luminescence,* Vol. 121, pp. 319-321, ISSN 0022-2313

Guillermain, E.; Lysenko, V.; Oroubtchouk, R.; Benyattou, T.; Roux, S.; Pillonnet, A. & Perriat, P. (2007). Bragg surface wave device based on PSi and its application for sensing. *Applied Physics Letters*, Vol.90, No. 24, pp. 241116, ISSN 0003-6951

Gurtner, C.; Wun, A.W. & Sailor, M.J. (1999). Surface modification of PSi by electrochemical reduction of organo halides. *Angewandte Chemie-International Edition,* Vol. 38, No. 13-14, pp. 1966-1968, ISSN 1433-7851

Jamois, C.; Li, C.; Orobtchouk, R. & Benyattou, T. (2010a). Slow Bloch surface wave devices on PSi for sensing applications. *Photonics and Nanostructures: Fundamentals and Applications*, Vol. 8, No. 2, pp. 72-77, ISSN 1569-4410

Jamois, C.; Li, C.; Gerelli, E.; Chevolot, Y.; Monnier, V.; Skryshevskyi, R.; Orobtchouk, R.; Souteyrand, E. & Benyattou, T. (2010b). Porous-silicon based planar photonic crystals for sensing applications, *Proceedings SPIE 7713, Conference on Photonic Crystal Materials and Devices IX*, 7713OU pp. 1-10, Brussels, Belgium, April 12-15, 2010, ISSN 0277-786X

Jane, A.; Dronov, R.; Hodges, A. & Völcker, N.H. (2009). Porous silicon biosensors on the advance. *Trends in Biotechnology*, Vol. 27, No. 4, pp. 230-239, ISSN 0167-7799

Joannopoulos, J.D.; Meade, R.D. & Winn, J.N. (1995). *Photonic crystals, molding the flow of light*. Princeton Academic Press, Princeton, NJ, ISBN 0-691-03744-2

Johnson, S.G., & Joannopoulos, J.D. (2001). Block-iterative frequency-domain methods for Maxwell's equations in a planewave basis. *Optics Express*, Vol. 8, No. 3, pp. 173-190, ISSN 1094-4087

Kim, N.Y. & Laibinis, P.E. (1998). Derivatization of PSi by Grignard reagents at room temperature. *Journal of the American Chemical Society,* Vol. 120, No. 18, pp. 4516-4517, ISSN 0002-7863

Kochergin, V. & Föll, H. (2009). *Porous Semiconductors Optical Properties and Applications*. Springer, ISBN 978-1-84882-577-2, London

Lehmann, V. & Gösele, U. (1991). Porous silicon formation: A quantum wire effect. *Applied Physics Letters*, Vol. 58, No. 8, pp. 856-858, ISSN 0003-6951

Lehmann, V.; Stengl, R. & Luigart, A. (2000). On the morphology and the electrochemical formation mechanism of mesoporous silicon. *Materials Science and Engineering*, Vol. B 69–70, pp. 11-22, ISSN 0921-5107

Lerondel, G.; Setzu, S.; Thönissen, M. & Romestain, R. (1997). Holography in PSi. *Journal of Imaging Science and Technology*, Vol. 41, No .5, pp. 468-473, ISSN 8750-9237

Lin, V.S.–Y.; Motesharei, K.; Dancil, K.-P.S.; Sailor, M.J. & Ghadiri, M.R. (1997). A porous silicon-based optical interferometric biosensor. *Science*, Vol. 278, pp. 840-842

Liscidini, M. & Sipe, J.E. (2007). Enhancement of diffraction for biosensing applications via Bloch surface waves. *Applied Physics Letters*, Vol. 91, pp. 253125, ISSN 0003-6951

Looyenga, H. (1965). Dielectric constants of heterogeneous mixtures. *Physica*, Vol. 31, pp. 401–406

Martin, J.R.; Souteyrand, E.; Lawrence, M.F. & Mikkelsen, S.R. (1994). Procedure for the analysis of biological substances in a conductive liquid medium (GENFET). 1994 French Patent n° 94 0868, US Patent Application: USSN 08/ 649,985

Mathew, F.P. & Alocilja, E.C. (2005) Porous silicon based biosensor for pathogen detection. *Biosensors and Bioelectronics*, Vol. 20, No. 8, pp. 1656-1661, ISSN 0956-5663

Meade, S.O. & Sailor, M.J. (2007). Microfabrication of freestanding PSi particles containing spectral barcodes, *Physica Status Solidi*, Vol. 1, No. 2, pp. R71–R73, ISSN 1862-6254

Moni, L.; Pourceau, G.; Zhang, J.; Meyer, A.; Vidal, S.; Souteyrand, E.; Dondoni, A.; Morvan, F.; Chevolot, Y.; Vasseur, J.-J. & Marra, A. (2009). Design of Triazole-Tethered Glycoclusters Exhibiting Three Different Spatial Arrangements and Comparative Study of their Affinities towards PA-IL and RCA 120 by Using a DNA-Based Glycoarray. *Chembiochem,* Vol. 10, No. 8, pp. 1369-1378, ISSN 1439-4227

Ouyang, H.; Striemer, C.C. & Fauchet, P.M. (2006). Quantitative analysis of the sensitivity of PSi optical biosensors. *Applied Physics Letters*, Vol. 88, pp. 163108, ISSN 0003-6951

Palik, E.D. (1998). *Handbook of optical constants of solids*. Academic Press New York, ISBN 0-12-544423-0

Park, H.; Dickerson, J.H; & Weiss, S.M. (2008). Spatially localized one-dimensional PSi photonic crystals. *Applied Physics Letters*, Vol. 92, No. 1, pp. 011113, ISSN 0003-6951

Phaner-Goutorbe, M.; Dugas, V.; Chevolot, Y. & Souteyrand, E. (2011). Silanization of silica and glass slides for DNA microarrays by Impregnation and Gas phase Protocols: A comparative study. *Material Science and Engineering C,* Vol. 31, No. 2, pp. 384-390, ISSN 0928-4931

Press, W.H.; Flannery, B.P.; Teukolsky, S.A. & Vetterling, W.T. (1992). *Numerical Recipes in C: The art of Scientific Computing*. Cambridge University Press, ISBN 0-521-43108-5

Rendina, I.; Rea, I.; Rotiroti, L. & De Stefano, L. (2007). Porous silicon-based optical biosensors and biochips. *Physica E*, Vol. 38, pp. 188-192, ISSN 1386-9477

Robins, E.G.; Stewart, M.P. & Buriak, J.M. (1999). Anodic and cathodic electrografting of alkynes on PSi. *Chemical Communications,* No. 24, pp. 2479-2480, ISSN 1359-7345

Rong, G.; Najmaie, A.; Sipe, J.E. & Weiss, S.M. (2008). Nanoscale PSi waveguide for label-free DNA sensing. *Biosensors and Bioelectronics,* Vol. 23, No. 10, pp. 1572-1576, ISSN 0956-5663

Rossi, A.M.; Wang, L.; Reipa, V & Murphy, T.E. (2007). Porous silicon biosensor for detection of virus. *Biosensors and Bioelectronics*, Vol. 23, pp. 741-745, ISSN 0956-5663

Ryckman, J.D.; Liscidini, M.; Sipe, J.E. & Weiss, S.M. (2010). PSi structures for low-cost diffraction-based biosensing. *Applied Physics Letters*, Vol. 96, pp. 171103

Sassolas, A.; Leca-Bouvier, B.D. & Blum, L.J. (2008). DNA Biosensors and Microarrays. *Chemical Reviews,* Vol. 108, No. 1, pp. 109-139, ISSN 00092665

Sedra, A.S. & Smith, K.C. (1997). *Microelectronics Circuits*. 4th Edition, Oxford University Press, ISBN 978-0195116632

Setzu, S.; Lerondel, G. & Romestain, R. (1998). Temperature effect on the roughness of the formation interface of p-type PSi. *Journal of Applied Physics*, Vol. 84, No. 6, pp. 3129-3133, ISSN 0021-8979

Shinn, M. & Robertson, W.M. (2005). Surface plasmon-like sensor based on surface electromagnetic waves in a photonic band-gap material. *Sensors and Actuators B*, Vol. 105, No. 2, pp. 360-364, ISSN 0925-4005

Sirbuly, D.J.; Lowman, J.M.; Scott, B.; Stucky, G.D & Buratto, S.K. (2003). Patterned microstructures of PSi by dry-removal soft lithography. *Advanced Materials*, Vol. 15, No. 2, pp. 149-152, ISSN 0935-9648

Song, M.-J.; Yun, D.-H.; Min, N.-K. & Hong, S.-I. (2006). Comparison of effective working electrode areas on planar and porous silicon substrates for Cholesterol Biosensor. *Japanese Journal of Applied Physics*, Vol. 45, N°9A, pp. 7197-7202, ISSN 0021-4922

Soref, R.A. & Bennett, B.R. (1987). Electrooptical effect in Silicon. *IEEE Journal of Quantum Electronics*, Vol. 23, pp. 123-129, ISSN 0018-9197

Soultani-Vigneron, S.; Dugas, V.; Rouillat, M.H.; Fedolliere, J.; Duclos, M.C.; Vnuk, E.; Phaner-Goutorbe, M.; Bulone, V.; Martin, J.R.; Wallach, J. & Cloarec, J.-P. (2005). Immobilisation of oligo-peptidic probes for microarray implementation: Characterisation by FTIR, Atomic Force Microscopy and 2D fluorescence. *Journal Of Chromatography B-Analytical Technologies In The Biomedical And Life Sciences,* Vol. 822, No. 1-2, pp. 304-310, ISSN 1570-0232

Souteyrand, E.; Cloarec, J.-P.; Martin, J.R.; Wilson, C; Lawrence, I.; Mikkelsen, S.R. & Lawrence, M.F. (1997). Direct detection of the hybridization of specific DNA sequences by field effect. *Journal of Physical Chemistry*, Vol. 101, No.15, pp.2980-2985

Souteyrand, E.; Chen, C.; Cloarec, J;-P.; Nesme, X.; Simonet, P.; Navarro, I. & Martin, J.R. (2000). Comparison between the electrochemical and optoelectrochemical impedance measurement for the detection of DNA hybridization. *Applied Biotechnology and Biochemistry*, Vol. 89, pp. 195-207, ISSN 0273-2289

Steinem, C.; Janshoff, A.; Lin, V.S.-Y.; Völcker, N.H. & Ghadiri, M.R. (2004). DNA hybridization-enhanced porous silicon corrosion: mechanistic investigations and prospect for optical interferometric biosensing. *Tetrahedron*, Vol. 60, pp. 11259, ISSN 0040-4020

Stewart, M.P. & Buriak, J.M. (2000). Chemical and Biological Applications of PSi Technology. *Advanced Materials,* Vol. 12, No. 12, pp. 859-869, ISSN 0935-9648

Taflove, A & Hagness, S.C. (2005). *Computational Electrodynamics: The Finite-Difference Time-Domain Method*. Third Edition, Artech House, Boston, ISBN 978-1-58053-832-9

Thévenot, D.R.; Roth, K.; Durst, R.A. & Wilson, G.S. (1999). Electrochemical biosensors: recommended definitions and classification. *Pure and Applied Chemistry,* Vol. 71, No. 12, pp. 2333-2348, ISSN 0033-4545

Thust, M.; Schöning, M.J; Frohnhoff, S.; Arens-Fischer, R.; Kordos, P. & Lüth, H. (1996). Porous silicon as a substrate material for potentiometric biosensors. *Measurements Science and Technology*, Vol. 7, pp. 26-29, ISSN 0957-0233

Thust, M.; Schöning, M.J; Schroth, P.; Malkoc, U.; Dicker, C.I.; Steffen, A.; Kordos, P. & Lüth, H. (1999). Enzyme immobilisation on planar and porous silicon substrates for biosensors applications. *Journal of molecular Catalysis B*, Vol.7, pp.77, ISSN 1381-1177

Tinsley-Bown, A.M.; Canham, L.T.; Hollings, M.; Anderson, M.H.; Reeves, C.L.; Cox, T.I.; Nicklin, S.; Squirrell, D.J.; Perkins, E.; Hutchinson, A.; Sailor, M.J. & Wun, A. (2000). Tuning the Pore Size and Surface Chemistry of PSi for Immunoassays. *Physica Status Solidi (a),* Vol. 182, No. 1, pp. 547-553, ISSN 0031-8965

Tserepi, A.; Tsamis, C.; Gogolides, E. & Nassiopoulou, A.G. (2003). Dry etching of PSi in high density plasmas, *Physica Status Solidi (a)*, Vol. 197, pp.163-167, ISSN: 0031-8965

Viktorovitch, P.; Drouard, E.; Garrigues, M..; Leclercq, J.-L.; Letartre, X.; Rojo-Romeo, P. & Seassal, C. (2007). Photonic crystals: basic concepts and devices. *Comptes Rendus Physique*, Vol.8, pp. 253-266

Viktorovitch, P.; Ben Bakir, B.; Boutami, S.; Leclercq, J.-L.; Letartre, X.; Rojo-Romeo, P.; Seassal, C.; Zussy, M.; Di Cioccio, L. & Fedeli, J.-M. (2010). 3D harnessing of light with 2.5D photonic crystals. *Laser & Photonics Reviews*, Vol.4, No.3, pp. 401–413

Völcker, N.H.; Alfonso, I. & Ghadiri, M.R. (2008). Catalyzed oxidative corrosion of porous silicon used as an optical transducer for ligand–receptor interactions. *ChemBioChem*, Vol.9, pp.1176-1186

Zhang, J.; Pourceau, G.; Meyer, A.; Vidal, S.; Praly, J.-P.; Souteyrand, E.; Vasseur, J.-J.; Morvan, F. & Chevolot, Y. (2009a). DNA-directed immobilisation of glycomimetics for glycoarrays application: Comparison with covalent immobilisation, and development of an on-chip IC50 measurement assay. *Biosensors and Bioelectronics,* Vol.24, No.8, pp. 2515, ISSN 0956-5663

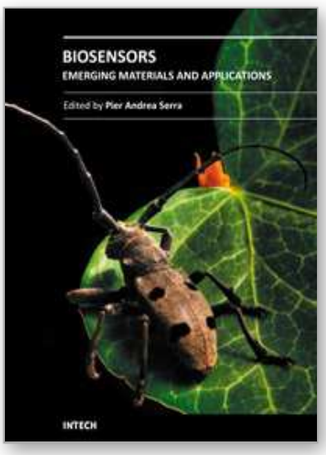

Biosensors - Emerging Materials and Applications

Edited by Prof. Pier Andrea Serra

ISBN 978-953-307-328-6
Hard cover, 630 pages
Publisher InTech
Published online 18, July, 2011
Published in print edition July, 2011

A biosensor is a detecting device that combines a transducer with a biologically sensitive and selective component. Biosensors can measure compounds present in the environment, chemical processes, food and human body at low cost if compared with traditional analytical techniques. This book covers a wide range of aspects and issues related to biosensor technology, bringing together researchers from 19 different countries. The book consists of 27 chapters written by 106 authors and divided in three sections: Biosensors Technology and Materials, Biosensors for Health and Biosensors for Environment and Biosecurity.

InTech Europe
University Campus STeP Ri
Slavka Krautzeka 83/A
51000 Rijeka, Croatia
Phone: +385 (51) 770 447
Fax: +385 (51) 686 166
www.intechopen.com

InTech China
Unit 405, Office Block, Hotel Equatorial Shanghai
No.65, Yan An Road (West), Shanghai, 200040, China
中国上海市延安西路65号上海国际贵都大饭店办公楼405单元
Phone: +86-21-62489820
Fax: +86-21-62489821

IntechOpen